This article was downloaded by: *[Haskel, Daniel]*
On: *28 September 2008*
Access details: *Access Details: [subscription number 903096108]*
Publisher *Taylor & Francis*
Informa Ltd Registered in England and Wales Registered Number: 1072954 Registered office: Mortimer House, 37-41 Mortimer Street, London W1T 3JH, UK

High Pressure Research
Publication details, including instructions for authors and subscription information:
http://www.informaworld.com/smpp/title~content=t713679167

Magnetic spectroscopy at high pressures using X-ray magnetic circular dichroism

Daniel Haskel [a]; Y. C. Tseng [a]; N. M. Souza-Neto [a]; J. C. Lang [a]; S. Sinogeikin [b]; Ya. Mudryk [c]; K. A. Gschneidner Jr [c]; V. K. Pecharsky [c]
[a] Advanced Photon Source, Argonne National Laboratory, Argonne, IL, USA [b] HPCAT - Carnegie Institution of Washington, Argonne, IL, USA [c] Materials and Engineering Physics Program, Ames Laboratory, Iowa State University, Ames, IA, USA

Online Publication Date: 01 September 2008

To cite this Article Haskel, Daniel, Tseng, Y. C., Souza-Neto, N. M., Lang, J. C., Sinogeikin, S., Mudryk, Ya., Gschneidner Jr, K. A. and Pecharsky, V. K.(2008)'Magnetic spectroscopy at high pressures using X-ray magnetic circular dichroism',High Pressure Research,28:3,185 — 192
To link to this Article: DOI: 10.1080/08957950802020307
URL: http://dx.doi.org/10.1080/08957950802020307

PLEASE SCROLL DOWN FOR ARTICLE

Full terms and conditions of use: http://www.informaworld.com/terms-and-conditions-of-access.pdf

This article may be used for research, teaching and private study purposes. Any substantial or systematic reproduction, re-distribution, re-selling, loan or sub-licensing, systematic supply or distribution in any form to anyone is expressly forbidden.

The publisher does not give any warranty express or implied or make any representation that the contents will be complete or accurate or up to date. The accuracy of any instructions, formulae and drug doses should be independently verified with primary sources. The publisher shall not be liable for any loss, actions, claims, proceedings, demand or costs or damages whatsoever or howsoever caused arising directly or indirectly in connection with or arising out of the use of this material.

High Pressure Research
Vol. 28, No. 3, September 2008, 185–192

Taylor & Francis
Taylor & Francis Group

Magnetic spectroscopy at high pressures using X-ray magnetic circular dichroism

Daniel Haskel[a]*, Y.C. Tseng[a], N.M. Souza-Neto[a], J.C. Lang[a], S. Sinogeikin[b], Ya. Mudryk[c], K.A. Gschneidner, Jr[c] and V.K. Pecharsky[c]

[a]*Advanced Photon Source, Argonne National Laboratory, Argonne, IL, USA;* [b]*HPCAT – Carnegie Institution of Washington, Argonne, IL, USA;* [c]*Materials and Engineering Physics Program, Ames Laboratory, Iowa State University, Ames, IA, USA*

(*Received 24 January 2008; final version received 25 February 2008*)

The imbalance in the electronic density of states between spin-up and spin-down electrons characteristic of ferro(ferri)-magnetic materials gives rise to X-ray magnetic circular dichroism (XMCD) in the absorption of circularly polarized X-rays with opposite helicity. These dichroic effects are largest near element-selective atomic resonances and can be used to probe ferro(ferri)-magnetic ordering with element- and electronic orbital-selectivity. We describe recent developments at the Advanced Photon Source that allow measurements of XMCD in a diamond anvil cell. We discuss the challenges associated with these measurements as well as their potential to further our understanding of complex magnetic materials.

Keywords: magnetism; X-ray magnetic circular dichroism; XMCD; synchrotron radiation; X-ray absorption

Downloaded By: [Haskel, Daniel] At: 16:53 28 September 2008

1. Introduction

Remarkable advances in synchrotron radiation sources during the past two decades have resulted in high-brilliance X-ray beams ideally suited to probe small sample volumes required for high-pressure experimentation. As a consequence of this, a large number of X-ray based techniques have been adapted for experiments in a diamond anvil cell (DAC). These include X-ray diffraction, X-ray emission spectroscopy (XES) and nuclear resonance X-ray scattering, all of which have already contributed handsomely to answering important questions on phase stability, phase composition, compressibility and electronic structure in the context of geoscience and materials science problems [1–3].

*Corresponding author. Email: haskel@aps.anl.gov

ISSN 0895-7959 print/ISSN 1477-2299 online
This material is published by permission of the Argonne National Laboratory, operated by U. Chicago Argonne, LLC, for the US Department of Energy under Contract No. DE-AC02-06CH11357. The U.S. Government retains for itself, and others acting on its behalf, a paid-up, non-exclusive, and irrevocable worldwide license in said article to reproduce, prepare derivative works, distribute copies to the public, and perform publicly and display publicly, by or on behalf of the Government.
DOI: 10.1080/08957950802020307
http://www.informaworld.com

High-pressure studies of magnetism are also of great interest due to the intimate connection between overlapping electronic orbitals and resultant spin configurations of participating electrons. Examples include crystal-field driven transitions between high-spin and low-spin states in transition metal oxides and loss of electron correlation effects (and related magnetic order) upon increasing electronic bandwidth in Mott–Hubbard insulators. Despite this intimate connection, X-ray probes of magnetic long-range order such as X-ray magnetic scattering (XMS) and X-ray magnetic circular dichroism (XMCD) have been used only sporadically in the past decade to study magnetism at high pressures [4]. Only recently, new efforts have taken place aimed at developing full capabilities for these techniques in DACs [5–9]. The primary challenge for non-resonant magnetic X-ray scattering, which can use relatively high energies ($\sim$20 keV) and hence minimize X-ray absorption in the diamond anvils, is its weak scattering cross section (six-to-eight orders of magnitude weaker than X-ray charge scattering) [10]. Despite the small cross section, the high brilliance of third generation synchrotron radiation sources coupled with focusing optics allows for non-resonance XMS experiments to be carried out in the DAC, especially to probe antiferromagnetic (AFM) ordering, where charge and magnetic scattering are separated in reciprocal space [5]. While large resonant enhancements to the XMS cross section can be achieved, typical resonant energies for magnetic elements of interest lie in the 5–10 keV energy range where anvil absorption is quite significant, and large scattering angles are needed to access a reasonably large volume of reciprocal space.

The XMCD technique also requires tuning the X-ray energy to selected atomic resonances in the 5–10 keV range, and hence its implementation entails minimizing X-ray absorption in the diamond anvils. Unlike X-ray scattering, XMCD measures the difference in the absorption coefficient of a magnetized sample for opposite X-ray helicities, which is commonly done using a transmission geometry. Therefore, angular acceptance requirements for the DAC are much less stringent than those of a resonant X-ray scattering experiment. XMCD also requires a brilliant source of circularly polarized (CP) X-rays such as those produced by third generation synchrotron radiation sources using specialized insertion devices or phase retarding (PR) optics. The XMCD technique is the technique of choice to study ferro(ferri)-magnetic materials, yielding element- and orbital-selective magnetization [11–13]. This is of great advantage in cases where more than one magnetic specie is present, and for elucidating the role of selected electronic orbitals in mediating magnetic interactions. Neutron scattering techniques probe the magnetic moment of all scattering atoms simultaneously, and the collimation of neutron beams is inadequate for DAC experiments. Similarly, SQUID magnetometry lacks element-specificity and is limited to lower applied pressures due to restrictions in sample environment. Other X-ray probes of magnetism include XES and nuclear resonance X-ray scattering (Mössbauer) spectroscopy. Unlike XMCD, XES is a probe of local magnetic moment and is not sensitive to magnetic ordering, while Mössbauer spectroscopy can only be applied to selected isotopes.

Downloaded By: [Haskel, Daniel] At: 16:53 28 September 2008

2. X-ray magnetic circular dichroism

X-ray absorption through the photoelectric effect involves the excitation of a bound, core electron (initial state) into unoccuppied electronic states (final state). Selection rules for electric-dipole transitions using linearly polarized light require that initial and final states differ by one unit of angular momentum $\Delta l = \pm 1$ in order to account for the lost angular momentum of the incident photon. The transition probability, given by Fermi's golden rule, depends on the unoccuppied density of states with the orbital character dictated by this selection rule, *i.e.* it is orbital-specific. When CP X-rays are used, additional selection rules come into place because the X-ray photon carries helicity, *i.e.* a well-defined projection of angular momentum along its propagation direction,

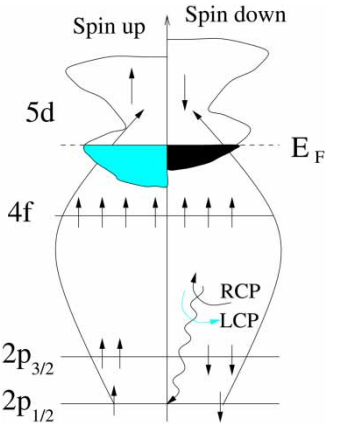

Figure 1. Schematic representation of the electronic transitions responsible for XMCD. The situation corresponds to the L_2 ($2p_{1/2}$) absorption edge in rare-earth Gd metal (half-filled 4f shell). The 5d band probed by this transition is split between spin-up and spin-down states by intra-atomic 4f–5d exchange.

Downloaded By: [Haskel, Daniel] At: 16:53 28 September 2008

$l_z = \pm 1$. If one neglects spin–orbit coupling in both initial and final states, this projection of angular momentum ought to be conserved in the absorption process, and it is transferred to the excited electron. However, in the presence of spin–orbit coupling in either the initial or final state, l_z is not a good quantum number (not conserved) while the total angular momentum $\mathbf{j} = \mathbf{l} + \mathbf{s}$, and its projection j_z, are. Under these conditions, the photon's projection of angular momentum is transferred to spin-polarization of the excited electrons. It can be shown that right-CP photons create spin-down photoelectrons, while left-CP photons create spin-up photoelectrons [14]. The photoelectron's spin-polarization is equal in magnitude but opposite in sign for opposite X-ray helicities. Since magnetic materials have an imbalance in the density of spin-up and spin-down unoccuppied electronic states (Figure 1), this gives rise to a difference in absorption cross section for opposite X-ray helicities – the XMCD. The size of the XMCD signal depends on both the spin-polarization of the photoelectron and the spin-polarization of the partial density of states probed by the selected dipole transition.

The largest dichroic effects are found in the soft X-ray regime where transition metal $L_{2,3}$ absorption edges ($2p \rightarrow 3d$ excitation) and rare-earth $M_{4,5}$ absorption edges ($3d \rightarrow 4f$ excitation) directly probe the (large) spin-polarization of electronic states carrying most of the material's magnetization (3d and 4f states, respectively). These resonances, however, are in the 0.5–1.5 keV energy range, and hence are incompatible with transmission experiments in the DAC (0.1 mm diamond thickness reduces the X-ray intensity by 12 orders of magnitude). The higher energies of transition metal K absorption edges ($1s \rightarrow 4p$) and rare-earth $L_{2,3}$ absorption edges ($2p \rightarrow 5d$), in the 5–9 keV range, are more suitable for XMCD experiments in a DAC (1.0 mm diamond thickness reduces the transmitted X-ray intensity by $\times 10$ at 7 keV). The challenge is that XMCD signals at these resonances are weak (0.1%–6%) due to the small induced spin-polarization in the 4p and 5d electronic states, and the lack of spin–orbit coupling in the 1*s* initial state of K-edge absorption. While these small XMCD signals are now routinely measured at a number of synchrotron radiation sources, the incorporation of a DAC environment with the concomitant increase in X-ray absorption presents more stringent requirements for an accurate measurement of XMCD.

It is also important to note that XMCD is a vectorial probe of magnetism. Since the photoelectron is spin-polarized along or opposite the X-ray helicity (X-ray propagation direction), the XMCD signal depends on the relative alignment of the X-ray wavevector and the quantization axis determined by an applied magnetic field $\hat{k} \cdot \hat{m}$, where $\hat{m}$ is the local moment direction. Since the

X-ray absorption process averages over many absorbing sites, the vectorial nature of XMCD implies that a *net* element-specific magnetization $\langle(\hat{k}\cdot\hat{m})\rangle \neq 0$ is required to yield an XMCD signal. Unlike XES or Mössbauer spectroscopy, XMCD is absent when local atomic moments are present but are oriented randomly relative to the incident photon wavevector. This is the situation in the paramagnetic state of ferromagnetic (FM) materials (above the Curie ordering temperature), where temperature fluctuations overcome the exchange interaction responsible for spin–spin correlations, and magnetic order is destroyed. XMCD is also absent when a ferromagnet spontaneously orders in a multiple domain structure with randomly oriented magnetic domains, as occurs in the absence of an applied magnetic field, unless the X-ray beam size is small enough to avoid averaging over the magnetic domains [15]. XMCD is also absent in antiferromagnets where no net magnetization is present. An applied magnetic field, however, may induce canting of the AFM spin structure and result in a net magnetic moment and non-zero XMCD signal [16]. Since magnetic ordering temperatures are determined by the strength of exchange interactions, and are known to not exceed ~1500 K, the vectorial nature of XMCD has implications for its applicability under P–T conditions relevant to the Earth sciences; *i.e.* it is limited to temperature conditions found in the upper mantle. Experimentally, the requirement of element-specific net magnetization implies the need for applied magnetic fields and, oftentimes, low-temperature capabilities.

Downloaded By: [Haskel, Daniel] At: 16:53 28 September 2008

3. Experimental

The key challenge for XMCD measurements in the DAC is the diamond anvil's absorption for X-ray energies in the 5–10 keV range. The anvil's absorption not only reduces the transmitted intensity affecting counting statistics critical for the detection of small dichroic signals, but also imposes more stringent demands on the degree of rejection of higher-energy harmonics present in the nominally monochromatic incident X-ray beam. These harmonics are preferentially transmitted through a highly absorbing DAC distorting the measurement of XMCD. To address this issue, we have incorporated perforated diamond anvils into our DAC. This configuration, which is similar to that reported in [17], is shown in the left panel of Figure 2. It involves a fully perforated anvil serving as backing plate for a 0.7 mm thick mini-anvil, and a partially perforated anvil with a 0.1 mm thick inner wall. The perforated anvils, which are manufactured by D'ANVILS (Tel Aviv), feature tapered perforations with entrance and exit dimensions of 1 and 0.1 mm,

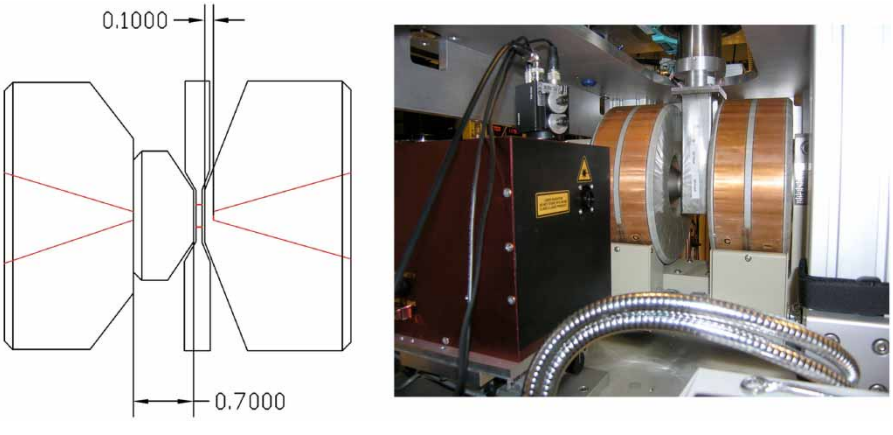

Figure 2. Left: Diamond anvil configuration featuring fully- and partially-perforated anvils for X-ray transmission in the 5–10 keV range. Right: Cryostat/DAC assembly shown in between the pole pieces of the electromagnet. Pressure is calibrated *in-situ* by translating the cryostat/DAC into the ruby fluorescence station on the side of the magnet.

respectively, resulting in an angular aperture of $\sim\pm 15°$. This angular aperture allows rotation of the DAC to remove unwanted Bragg diffraction in the diamond anvils, were it to appear during energy scans (± 50 eV) through the element-specific absorption edges.

While the asymmetric configuration is more costly and results in a larger diamond thickness than could be achieved with two partially-perforated anvils, this configuration retains a smooth optical surface on the mini-anvil side allowing for *in-situ* pressure calibration using the ruby fluorescence method (partial perforation results in a rough inner surface). While *in-situ* pressure calibration using the X-ray absorption fine structure (XAFS) technique [9] does not require smooth optical surfaces and can be used with a symmetric anvil configuration involving two partially-perforated anvils, this method is more time consuming than the standard ruby method as it requires extended energy XAFS scans through the absorption edge of the calibrant material. In addition, the XAFS data are more likely to be affected by Bragg diffraction in the diamond anvils due to the extended energy range, although this problem can be mitigated by collecting XAFS data at two different angular positions of the DAC [9].

The total diamond thickness, of ~ 0.8 mm, reduces the transmitted X-ray intensity by a factor of about six at 7 keV. Compatibility with applied magnetic fields and low temperatures is met by using a non-magnetic, copper–beryllium piston–cylinder DAC (model WCM-7B manufactured by easyLab Technologies Ltd.). The He-gas membrane cell allows an *in-situ* change of pressure under cryogenic conditions. The CuBe DAC is in thermal contact with the cold finger of a He-flow refrigerator for low-temperature measurements. The cryostat is mounted in high resolution translation stages for sample scanning and placed between the (hollowed) pole pieces of an electromagnet. The magnet delivers a 0.6 Tesla magnetic field at the sample position, directed along the X-ray propagation direction. Pressure calibration is achieved by a motorized translation of the DAC/cryostat assembly from the center of the magnet to the ruby fluorescence calibration system located on the side of the magnet, shown in the right panel of Figure 2.

CP X-rays are generated using PR diamond optics [18,19]. The advantage of PR optics over specialized insertion devices, such as helical undulators, is the ability to quickly switch X-ray helicity (switching frequency 10–20 Hz), enabling the use of lock-in detection of the small dichroic signals [20]. Helicity switching is achieved by offseting a diamond (1 1 1) crystal away from its Bragg condition using a piezoelectric actuator. A square waveform with the required peak-to-peak voltage V_{pp} and selected frequency is used to alternate between opposite X-ray helicities, and the related modulation in the absorption coefficient (XMCD) is detected with a phase lock-in amplifier. This allows XMCD signals as small as 10 ppm to be detected. The beamline is equipped with a set of toroidal (Pd) and flat (Si) mirrors for X-ray focusing and harmonic rejection, respectively. Additional details on beamline optics and flux conditions can be found in [9,21].

4. Application to magnetocaloric material $Gd_5(Si_xGe_{1-x})_4$

To illustrate the potential of this technique to our further understanding of complex magnetic materials, we present results on a new class of magnetocaloric materials, namely $Gd_5(Si_xGe_{1-x})_4$ ternary alloys. These materials have attracted attention because they display a first-order magneto-structural transition that can be triggered with an applied magnetic field [22–26]. The large field-induced changes in magnetic and structural entropy associated with this (otherwise second order) paramagnetic-to-FM, first-order transition result in a giant magneto-caloric effect that can be harnessed for magnetic refrigeration applications. Key to this effect is the emergence of FM ordering with Si doping from within the AFM ordering of the Gd_5Ge_4 parent compound. Since replacing Ge ions with the smaller Si ions leads to a contraction of the crystal lattice (chemical pressure) and stabilizes FM ordering (Curie temperature T_c increases with Si doping),

Downloaded By: [Haskel, Daniel] At: 16:53 28 September 2008

it is commonly assumed that the volume contraction plays a role in enhancing the Gd–Gd FM exchange – over the Gd–Gd AFM exchange – interactions. Since the Gd 4f spins are localized on their atomic sites with no overlap of 4f wavefunctions between different Gd sites, the exchange interactions are indirect and mediated by the spin-polarization of the hybridized Gd 5d– Ge 4p– Si 3p wavefunctions which make up the conduction band of these materials. A volume reduction may change the overlap of these wavefunctions and hence their ability to mediate exchange between localized Gd 4f spins. In order to test this theory and separate the effect of a macroscopic volume contraction from other electronic/local structure effects introduced with Si doping, we carried out high-pressure XMCD experiments in the DAC.

Finely ground powders of a Ge-rich $Gd_5(Si_{0.0375}Ge_{0.9625})_4$ alloy were mixed with silicon oil pressure-transmitting medium. Cu fine powders were added to the mixture to enable pressure calibration through measurement of Cu XAFS [9]. The volume ratio of sample, calibrant and pressure-medium was ∼1:1:15 in order to yield sample and calibrant absorption $\mu t \sim 1$ to 2 above the Gd L_3- and Cu K- absorption edges (μ is the linear absorption coefficient and t is effective thickness). Finely ground ruby powder was added onto the face of the mini-anvil for pressure calibration using the ruby fluorescence method. The mixture was loaded into the 250 μm hole of a stainless steel gasket that was preindented to 80 μm. Diamond culet size was 600 μm. Gas ionization chambers were used to detect the incident (I_0) and transmitted (I_t) intensities. The XMCD data were collected by modulating the X-ray helicity at 12.7 Hz and detecting the related modulation in absorption coefficient $\mu t = \ln(I_0/I_t)$ with a lock-in amplifier. The applied magnetic field was 0.6 Tesla.

Figure 3 shows the XMCD raw data at the Gd L_3 absorption edge at 35 K (top), its temperature-dependent integrated area (bottom, left) and the XMCD saturation value (35 K) for various applied

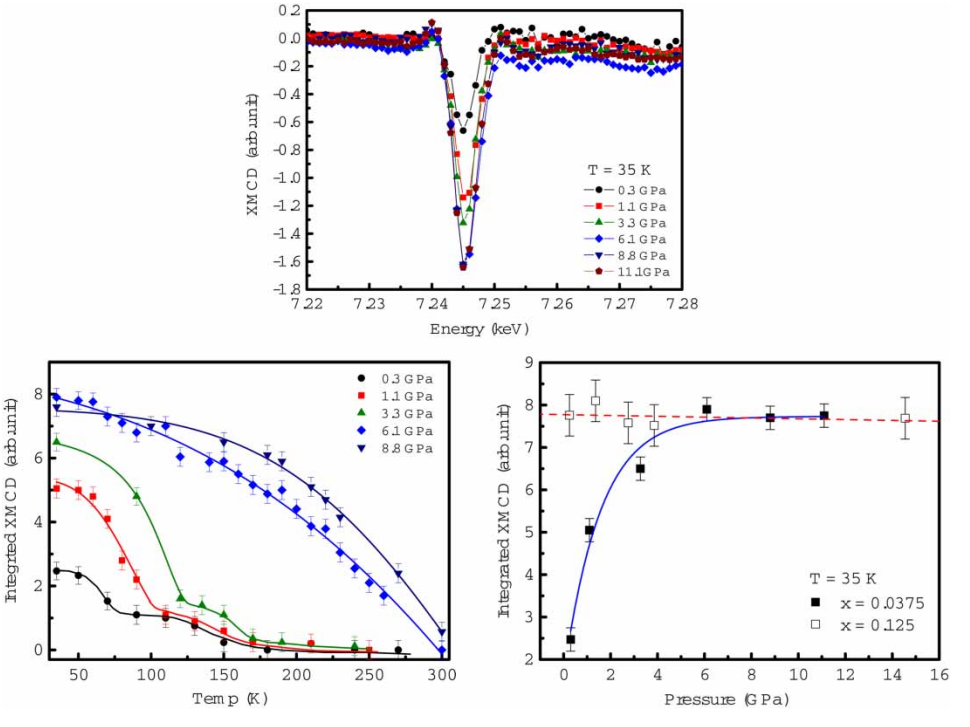

Figure 3. Top: XMCD data at the Gd L_3 absorption edge for various pressures and $T = 35$ K. Bottom, left: temperature-dependence of integrated XMCD intensity at various pressures. Bottom, right: saturation magnetization (35 K) as a function of pressure for $x = 0.0375$ and $x = 0.125$ samples.

Downloaded By: [Haskel, Daniel] At: 16:53 28 September 2008

pressures below 12 GPa. The temperature-dependent data show the presence of two magnetic transitions below 6 GPa and only one magnetic transition above 6 GPa. The first transition, which remains at high pressures, shows a large drop in magnetization and strong pressure dependence. The second transition features a small drop in magnetization, a weak dependence on pressure, and is absent above 6 GPa. By comparing with the (x, T) phase diagram [22], we assign the first transition to a FM-AFM transition with T_c shifting linearly with pressure from ~60 K at 0.3 GPa to ~250 K at 8.8 GPa. The shift in FM Curie temperature with pressure of dT_c/dP ~22 K GPa^{-1} is in reasonable agreement with values of 12 and 30 K GPa^{-1} reported in [16] and [24] for samples with $x = 0.125$ and $x = 0.1$, respectively. The second transition is assigned to an AFM–paramagnetic transition with transition temperature T_N ~130–150 K. The non-zero XMCD signal in the AFM phase is a result of canting of the AFM moments induced by the 0.6 Tesla applied magnetic field [16]. Since the same magnetic behavior observed by a pressure-induced volume reduction is observed by Si doping, namely a linear increase of FM T_c and the disappearance of the FM–AFM transition, it follows that the volume contraction introduced with Si doping is at least partially responsible for stabilizing FM order in this material. Further evidence for this is the behavior of the saturation magnetization as a function of pressure, shown in the right panel of Figure 3. The reduced saturation magnetization near ambient pressure is indicative of competing FM and AFM interactions in the $x = 0.0375$ sample. A volume reduction, introduced by pressure, stabilizes FM interactions and results in a saturation magnetization characteristic of samples with higher Si doping, such as with $x = 0.125$, where FM order is stable.

Downloaded By: [Haskel, Daniel] At: 16:53 28 September 2008

Acknowledgements

Work at Argonne and Ames is supported by the US Department of Energy, Office of Science, under Contract Nos. DE-AC-02-06CH11357 and DE-AC02-07CH11358, respectively. The authors would like to thank Dr A.O. Tsokol for providing some of the samples, and Drs Valentin Iota and Yang Ding for helpful discussions.

References

[1] M. Murakami, K. Hirose, K. Kawamura, N. Sata, and Y. Ohishi, Science 304 (2004), p. 855.
[2] J.-F. Lin, V.V. Struzhkin, S.D. Jacobsen, M.Y. Hu, P. Chow, J. Kung, H. Liu, H.-K. Mao, and R.J. Hemley, Nature 436 (2005), p. 377.
[3] W.L. Mao, H.-K. Mao, W. Sturhahn, J. Zhao, V.B. Prakapenka, Y. Meng, J. Shu, Y. Fei, and R.J. Hemley, Science 28 (2006), p. 564.
[4] F. Baudelet, J.M. Dubuisson, C. Hébert, C. Créoff, L. Pointal, R. Andouard, S. Odin, E. Dartyge, G. Krill, C.H. Giorgetti, J.C. Chervin, J.P. Itié, A. Polian, A. Fontaine, S. Pizzini, and J.P. Kappler, J. Synchrotron Rad. 5 (1998), p. 992.
[5] Y. Feng, R. Jaramillo, G. Srajer, J.C. Lang, Z. Islam, M.S. Somayazulu, O.G. Shpyrko, J.J. Pluth, H.-K. Mao, E.D. Isaacs, G. Aeppli, and T.F. Rosenbaum, Phys. Rev. Lett. 99 (2007), p. 137201.
[6] E. Duman, M. Acet, E.F. Wassermann, J. P. Itié, F. Baudelet, O. Mathon, and S. Pascarelli, Phys. Rev. Lett. 94 (2005), p. 075502.
[7] N. Ishimatsu, H. Maruyama, N. Kawamura, M. Suzuki, Y. Ohishi, M. Ito, S. Nasu, T. Kawakami, and O. Shimomura, J. Phys. Soc. Jpn. 72 (2003), p. 2372.
[8] V. Iota, J.-H. Park, C.-S. Yoo, J.C. Lang, D. Haskel, and G. Srajer, Appl. Phys. Lett. 90 (2007), p. 042505.
[9] D. Haskel, Y.C. Tseng, J.C. Lang, S. Sinogeikin, Rev. Sci. Instrum. 78 (2007), p. 083904.
[10] M. Blume and D. Gibbs, Phys. Rev. B 37 (1988), p. 1779.
[11] G. Schütz *et al.*, Phys. Rev. Lett. 58 (1987), p. 737.
[12] P. Carra and M. Altarelli, Phys. Rev. Lett. 64 (1990), p. 1286.
[13] J. Stöhr, J. Magn. Magn. Mater. 200 (1999), p. 470.
[14] U. Fano, Physical Review 178 (1969), p. 131.
[15] A. Cady, D. Haskel, J. Lang, G. Srajer, P. Chupas, R. Osborn, J.F. Mitchel, J.S. Ahn, N. Hur, S. Park, and S.-W. Cheong, Rev. Sci, Instrum. 76 (2005), p. 063702.
[16] Y.C. Tseng, D. Haskel, J.C. Lang, S. Sinogeikin, Y.A. Mudryk, V.K. Pecharsky, and K.A. Gschneidner, Jr., Phys. Rev. B 76 (2007), p. 014411.
[17] A. Dadashev, M.P. Pasternak, G. Kh. Rozenberd, and R.D. Taylor, Rev. Sci. Instrum. 72 (2001), p. 2633.

[18] K. Hirano, K. Izumi, T. Ishikawa, S. Annaka, and S. Kikuta, Jpn. J. Appl. Phys. Part 2 30 (1991), p. L407.
[19] J.C. Lang and G. Srajer, Rev. Sci. Instrum. 66 (1995), p. 1540.
[20] M. Suzuki, N. Kawamura, M. Mizumaki, A. Urata, H. Maruyama, S. Goto, and T. Ishikawa, Jpn. J. Appl. Phys. Part 2 37 (1998), p. L1488.
[21] J.W. Freeland, J.C. Lang, G. Srajer, R. Winarski, D. Shu, and D.M. Mills, Rev. Sci. Instrum. 73 (2002), p. 1408.
[22] V.K. Pecharsky and K.A. Gschneidner, Jr., Adv. Mater. (Weinheim, Ger.) 13 (2001), p. 683.
[23] F.-J. Perez-Reche, F. Casanova, E. Vives, L. Manosa, A. Planes, J. Marcos, X. Batelle, and A. Labarta, Phys. Rev. B 73, (2006), 014110.
[24] L. Morellon, Z. Arnold, P.A. Algarabel, C. Magen, M.R. Ibarra, and Y. Skorokhod, J. Phys. Condens. Matter 16 (2004), p. 1623.
[25] V.K. Pecharsky, A.P. Holm, K.A. Gschneidner, Jr., and R. Rink, Phys. Rev. Lett. 91 (2003), p. 197204.
[26] A.M.G. Carvalho, C.S. Alves, A. de Campos, A.A. Coelho, S. Gama, F.C.G. Gandra, P.J. van Ranke, and N.A. Oliveira, J. Appl. Phys. 97 (2005), p. 10M320.

Downloaded By: [Haskel, Daniel] At: 16:53 28 September 2008